Development 136, 3173-3183 (2009) doi:10.1242/dev.028902

Tbx1 controls cardiac neural crest cell migration during arch artery development by regulating *Gbx2* expression in the pharyngeal ectoderm

Amélie Calmont[1], Sarah Ivins[1], Kelly Lammerts Van Bueren[1], Irinna Papangeli[1], Vanessa Kyriakopoulou[1], William D. Andrews[2], James F. Martin[3], Anne M. Moon[4], Elizabeth A. Illingworth[5], M. Albert Basson[6] and Peter J. Scambler[1,*]

Elucidating the gene regulatory networks that govern pharyngeal arch artery (PAA) development is an important goal, as such knowledge can help to identify new genes involved in cardiovascular disease. The transcription factor Tbx1 plays a vital role in PAA development and is a major contributor to cardiovascular disease associated with DiGeorge syndrome. In this report, we used various genetic approaches to reveal part of a signalling network by which Tbx1 controls PAA development in mice. We investigated the crucial role played by the homeobox-containing transcription factor Gbx2 downstream of Tbx1. We found that PAA formation requires the pharyngeal surface ectoderm as a key signalling centre from which Gbx2, in response to Tbx1, triggers essential directional cues to the adjacent cardiac neural crest cells (cNCCs) en route to the caudal PAAs. Abrogation of this signal generates cNCC patterning defects leading to PAA abnormalities. Finally, we showed that the Slit/Robo signalling pathway is activated during cNCC migration and that components of this pathway are affected in *Gbx2* and *Tbx1* mutant embryos at the time of PAA development. We propose that the spatiotemporal control of this tightly orchestrated network of genes participates in crucial aspects of PAA development.

KEY WORDS: Pharyngeal arch arteries, Cardiac neural crest, Slit/Robo, Mouse

INTRODUCTION

The pharyngeal apparatus is a transient embryonic structure present during vertebrate development. It forms gradually as the pharynx segments into a series of arches and pouches in a cranial-to-caudal order. Each pharyngeal arch (PA) possesses an outer pharyngeal surface ectoderm (PSE) layer and an inner pharyngeal endodermal (P.endo) layer. In the centre of each PA, the pharyngeal arch artery (PAA) is encircled by a mesodermal core structure surrounded by a layer of neural crest cells (NCCs). The bi-lateral PAA system develops sequentially as the pharynx segments and allows blood to flow from the heart tube to the dorsal aortae (DeRuiter et al., 1993). At E10.5, five PAAs have formed, and whereas PAAs 1 and 2 have regressed into capillary beds, PAAs 3, 4 and 6 persist in their respective PAs. Starting from E11.5, these caudal PAAs undergo an extensive asymmetrical remodelling and persist later as parts of the great vessels arising from the aorta (Srivastava and Olson, 2000). Defective development of the fourth PAAs is responsible for severe vascular anomalies, such as interrupted aortic arch type B, which is postnatally lethal (Vitelli et al., 2002a). Perturbation of normal pharyngeal development is a feature of congenital diseases, such as DiGeorge syndrome, in which the main cause of death is congenital heart defects (CHDs) (Lindsay, 2001).

[1]Molecular Medicine Unit, Institute of Child Health, 30 Guilford Street, London WC1N 1EH, UK. [2]Department of Cell and Developmental Biology, University College London, London WC1E 6BT, UK. [3]Institute of Biosciences and Technology, Texas A&M Health Science Center, Houston, TX 77030, USA. [4]Departments of Pediatrics, Neurobiology and Anatomy and Human Genetics, University of Utah, Salt Lake City, UT 84112, USA. [5]Dulbecco Telethon Institute, c/o Telethon Institute of Genetics and Medicine, Via Pietro Castellino 111, 80131 Napoli, Italy. [6]Department of Craniofacial Development, King's College London, Floor 27, Guy's Tower, London SE1 9RT, UK.

*Author for correspondence (p.scambler@ich.ucl.ac.uk)

Accepted 16 July 2009

Haploinsufficiency of the T-box transcription factor *TBX1* is responsible for many features of DiGeorge syndrome (Paylor et al., 2006; Stoller and Epstein, 2005; Yagi et al., 2003). *Tbx1* is expressed dynamically in the developing pharyngeal apparatus in the mouse embryo and *Tbx1* homozygous mutants display severe cardiovascular, craniofacial, thymic, parathyroid and ear defects (Jerome and Papaioannou, 2001; Lindsay et al., 1999; Merscher et al., 2001). In particular, CHDs found in *Tbx1* mutant embryos consist of great vessel disruptions arising from defective fourth PAA development (Jerome and Papaioannou, 2001; Lindsay et al., 2001), and/or septation and alignment defects of the outflow tract (OFT) of the heart (Jerome and Papaioannou, 2001; Merscher et al., 2001). The essential role of Tbx1 in pharynx organogenesis relies on its ability to interact with crucial signalling pathways during development, such as the fibroblast growth factor (Fgf) (Hu et al., 2004; Vitelli et al., 2002b; Xu et al., 2004), hedgehog (Yamagishi et al., 2003) and retinoic acid (Guris et al., 2006; Roberts et al., 2006) signalling pathways. Furthermore, Tbx1 is required at different times (Xu et al., 2005), in different tissues (Arnold et al., 2006; Xu et al., 2005; Zhang et al., 2005; Zhang et al., 2006) and at different levels (Liao et al., 2004; Zhang and Baldini, 2008) to pattern all pharyngeal-derived structures. Thus, the analysis of Tbx1 effectors during embryonic development should advance our understanding of how the pharyngeal apparatus develops and, furthermore, aid in the identification of essential genes implicated in CHDs.

The special predisposition of the fourth PAA system toward interruption and/or hypoplasia is linked to the unique vascular morphology of these arteries (Bergwerff et al., 1999). Lineage-tracing in the mouse combined with morphological analysis of specific arterial segments has shown that muscular and non-muscular components of the fourth PAA system originate from cNCCs (Bergwerff et al., 1999; Jiang et al., 2000). cNCCs are pluripotent embryonic cells derived from the neuroepithelium (Le Douarin and Kalcheim, 1999). They originate from the neural folds in a region

between the middle of the otic vesicle and the caudal edge of somite 3 (Kirby et al., 1985). They migrate through PA 3, 4 and 6 (Miyagawa-Tomita et al., 1991) and form the vascular smooth muscle layer of these arteries (Le Lievre and Le Douarin, 1975). cNCCs also contribute to the connective tissue of the thymus, parathyroid and thyroid glands (Bockman and Kirby, 1984; Le Lievre and Le Douarin, 1975) and are essential for the formation of the aorticopulmonary septum (Kirby et al., 1983). cNCCs migrate long distances and, like NCCs in general, are extremely sensitive to external signalling from adjacent tissues, enabling them to interact with, and respond to, their changing milieu (Trainor and Krumlauf, 2000). Deletion of genes involved in cNCC migration (Feiner et al., 2001), self-renewal (Teng et al., 2008), survival (Macatee et al., 2003) and patterning (High et al., 2007), or ablation of premigratory cNCCs in the chick (Nishibatake et al., 1987), results in defective organogenesis of the PAA system. Therefore, the development of certain DiGeorge-like syndromic features, including great-artery defects, result, at least in part, from defective development of the cNCC lineage.

Notably, whereas *Tbx1* is expressed as early as E7.5 in all three germ layers (Chapman et al., 1996), it is not expressed in cNCCs (Garg et al., 2001); thus, the effects of *Tbx1* on cNCCs in fourth PAA development are non-cell-autonomous. Endothelial cells lining the fourth PAAs derive from mesodermal cells (Kirby and Waldo, 1995) and *Tbx1*-fated cells are found in the endothelium of the fourth PAA (Vitelli et al., 2002a; Zhang et al., 2005). Nevertheless, conditional deletion of *Tbx1* in endothelial cells does not generate fourth PAA defects (Zhang et al., 2005). Conditional deletion of *Tbx1* from all mesodermal expression domains has a severe impact on pharynx segmentation, with loss of PAs 3 to 6 and consequent developmental failure of the PAA system (Zhang et al., 2006). However, mesoderm-specific restoration of *Tbx1* expression in a mutant background rescues most of these defects, but not fourth PAA formation (Zhang et al., 2006). Subsequently, the PSE and P.endo, both of which express *Tbx1*, have been shown to be required for fourth PAA development (Arnold et al., 2006; Zhang et al., 2005). Also, the PSE has been shown to be a crucial source of Fgf signals for fourth PAA formation and remodelling (Macatee et al., 2003).

Although the diverse spatiotemporal functions of Tbx1 have been extensively studied and characterised, less is known about the genetic networks regulated by this protein during specific aspects of pharynx and heart development. Our laboratory and others have started to investigate potential downstream Tbx1 targets by analysing gene expression arrays obtained using available mouse models (Ivins et al., 2005; Liao et al., 2008). In this report, we provide new insights into how Tbx1 regulates important aspects of fourth PAA development by controlling the expression of the homeobox gene *Gbx2*. We employed a genetic approach to abrogate *Gbx2* activity downstream of Tbx1 and analysed resulting morphological and molecular defects. These studies revealed abnormalities in cNCC migration that lead to defective development of the PAAs and we propose a new mechanism by which Tbx1/Gbx2 might regulate cNCC migration via the Slit/Robo signalling pathway.

MATERIALS AND METHODS

Mutant mouse breeding and genotyping

The mouse lines used in this study have been described previously: $Tbx1^{+/-}$ (Lindsay et al., 2001), $Tbx1^{neo2/+}$ (Zhang et al., 2006), $Tbx1^{flox/flox}$ (Arnold et al., 2006; Xu et al., 2004); $Tbx1^{Cre}$ (Brown et al., 2004), $Gbx2^{+/-}$ (Wassarman et al., 1997), $Gbx2^{flox/flox}$ (Li et al., 2002), $AP2\alpha^{IresCre}$ (referred to as $AP2\alpha^{Cre}$ in the text) (Macatee et al., 2003), $Slit2^{+/-}$ (Plump et al., 2002) and R26R (Soriano, 1999). $Tbx1^{+/-}$, $AP2\alpha^{Cre}$ and $Tbx1^{neo2/+}$ lines were maintained on a C57Bl/6 background. $Tbx1^{Cre}$, $Gbx2^{+/-}$ and $Gbx2^{flox/flox}$ founders used in the crosses described below came originally from three different unknown, mixed backgrounds.

$Tbx1^{Cre/+};Gbx2^{flox/-}$ were generated by crossing $Tbx1^{Cre/+};Gbx2^{+/-}$ animals to $Gbx2^{flox/flox}$. Likewise, $AP2\alpha^{Cre/+};Gbx2^{+/-}$ animals were crossed to $Gbx2^{flox/flox}$ to generate *Gbx2-PSE* conditional mutant embryos: $AP2\alpha^{Cre/+};Gbx2^{flox/-}$. Finally, two types of *Tbx1-PSE* conditional mutants were generated: $AP2\alpha^{Cre/+};Tbx1^{+/-}$ animals were crossed to $Tbx1^{flox/flox}$ to generate $AP2\alpha^{Cre/+};Tbx1^{flox/-}$ and $AP2\alpha^{Cre/+};Tbx1^{+/flox}$ animals were crossed to $Tbx1^{flox/flox}$ to generate $AP2\alpha^{Cre/+};Tbx1^{flox/flox}$. $Fgf8^{neo/\Delta 2,3}$ embryos were obtained by crossing $Fgf8^{\Delta 2,3/+}$ mice with $Fgf8^{neo/+}$ mice and were genotyped as described (Meyers et al., 1998).

Real-time quantitative PCR

lacZ-expressing cells from E9.5 $Df1^{+/-};Tbx1^{+/-}$, effectively $Tbx1^{-/-}$ (Lindsay et al., 1999), and $Tbx1^{+/-}$ embryos were labelled using the CMFDG Labelling Kit (Molecular Probes) and collected by FACS. RNA was isolated using Trizol and amplified by PCR using the Microarray Target Amplification Kit (Roche). Quantitative real-time PCR was carried out on an ABI7000 and expression values were obtained using DART-PCR Analysis Excel software (Peirson et al., 2003). *Slit2* relative expression corresponds to n=3 technical replicates. Each sample represents cells collected from at least 10 E9.5 embryos.

RNA in situ hybridisation, ink injection and histological analysis

Whole-mount RNA in situ hybridisation was performed based on methods described previously (Wilkinson, 1992) using digoxygenin-labelled probes for *Gbx2*, *Slit1*, *Slit2*, *Slit3*, *Robo1* and *Sox10*. Ink injection was performed on E10.5 embryos fixed in 4% paraformaldehyde overnight at 4°C by targeting the OFT with a microinjection needle filled with Indian ink (Pélican). Mixed-stage embryos were stained with X-Gal following standard procedures (Nagy et al., 2003). Lysotracker Red (Invitrogen) was used at 5 μM for 20-30 minutes at 37°C. Anti-PECAM antibody (Mec13:3, Pharmingen) was used at 1:50, anti-Tbx1 antibody (Zymed) at 1:50, anti-GFP antibody (Sigma G6539) at 1:100 and anti-AP2α (Tcfap2α) antibody at 1:25 (3B5, Developmental Studies Hybridoma Bank). Whole-mount immunolabelling was carried out as described (Schwarz et al., 2008) using anti-p75 or anti-HNK-1 IgM antibody (Zymed MHCD 5701) at 1:100. Anti-Robo1 antibody was used at 1:2000 (Tamada et al., 2008) and signal was detected using biotinylated secondary antibody coupled with Streptavidin Alexa Fluor 488 conjugate. Alexa Fluor-conjugated secondary antibodies (Molecular Probes) were used at 1:200.

RESULTS

Gbx2 displays *Tbx1*-dependent expression domains

Loss of *Gbx2* is associated with abnormal development of the PAAs and hindbrain (Byrd and Meyers, 2005; Wassarman et al., 1997). In order to investigate whether Gbx2 could mediate some of the functions of Tbx1 during fourth PAA development, as previously suggested (Ivins et al., 2005), we compared *Gbx2* and *Tbx1* expression in wild-type (wt) and $Tbx1^{-/-}$ mouse embryos at E8.5, the specific time at which Tbx1 is required to pattern the PAAs (Xu et al., 2005). As shown in Fig. 1, both *Tbx1* and *Gbx2* are strongly expressed in the pharyngeal region of E8.5 wt embryos (Fig. 1A,D). Section analysis showed that *Gbx2* is expressed predominantly in the PSE, although some staining could also be detected in the P.endo (Fig. 1B). *Tbx1* and *Gbx2* expression overlap in these two epithelial domains [Fig. 1B,E, PSE (red arrow), P.endo (yellow arrow)], which are both potentially involved in PAA development (Zhang et al., 2005). *Tbx1* was additionally detected in the head mesoderm and in the secondary heart field (SHF) mesoderm, neither of which expressed *Gbx2* (Fig. 1B,E). From these observations, we conclude that *Gbx2* and *Tbx1* show overlapping expression domains at the time of fourth PAA specification. Later in development, *Tbx1* and

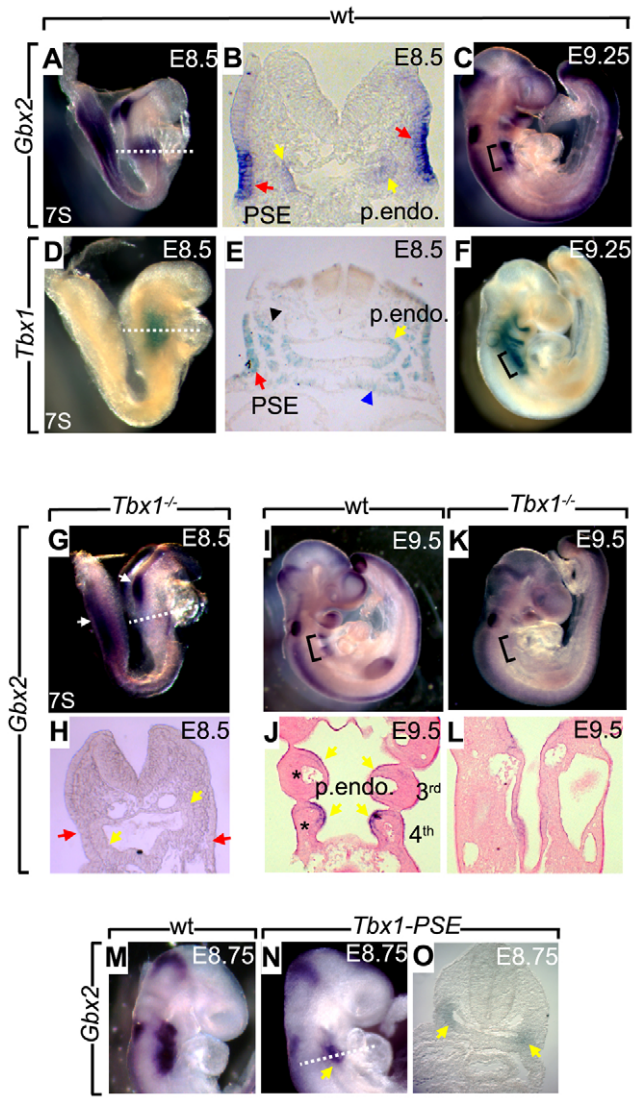

Fig. 1. *Gbx2* is downregulated in the pharyngeal epithelium of *Tbx1*$^{-/-}$ mouse embryos at the time of fourth PAA specification. (**A-O**) In situ hybridisation (ISH) for *Gbx2* on wild-type (wt) embryos (A-C,I,J,M), *Tbx1*$^{-/-}$ embryos (G,H,K,L), *Tbx1-PSE* (*AP2α*$^{Cre/+}$;*Tbx1*$^{flox/flox}$) embryos (N,O) and β-galactosidase staining of *Tbx1*$^{+/-}$ embryos (D-F). Dotted lines in A,D,G,N show section plane in B,E,H,O, respectively. Bracketed regions in C,F,I,K are the future location of caudal arches 3 to 6. Red and yellow arrows indicate regions of *Gbx2* and *Tbx1* staining in the PSE and in the P.endo, respectively. Black arrowhead indicates *Tbx1* expression in the head mesoderm; blue arrowhead indicates *Tbx1* expression in the SHF mesoderm.

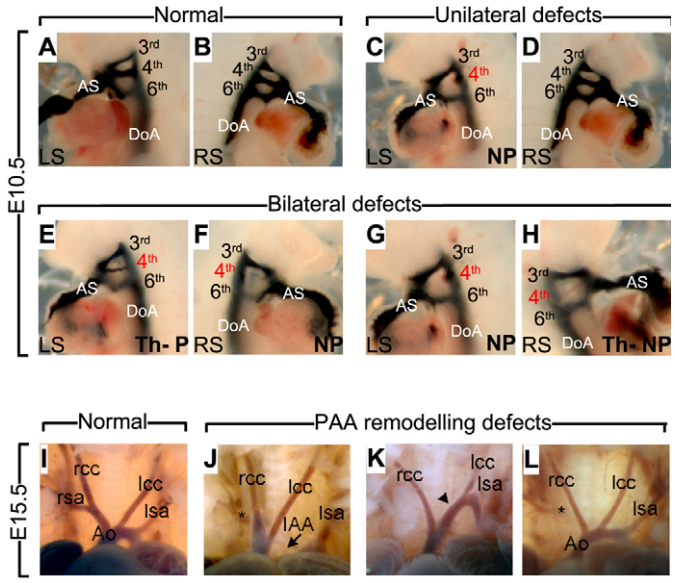

Fig. 2. *Gbx2* and *Tbx1* interact genetically in the development of the fourth PAA. Intracardiac ink injection of E10.5 (A-H) and frontal views of E15.5 (I-L) mouse embryos. (**A-H**) Fourth PAA defects in *Gbx2*$^{+/-}$, *Tbx1*$^{+/-}$ and *Gbx2*$^{+/-}$;*Tbx1*$^{+/-}$ embryos including non-patent to ink (NP), thin and patent to ink (Th-P) or thin and non-patent to ink (Th-NP). (**I-L**) Remodelling defects of the fourth PAA in E15.5 *Gbx2*$^{+/-}$;*Tbx1*$^{+/-}$ embryos (J-L) compared with wt embryo (I). (J) Interrupted arch type B (IAA, black arrow) combined with aberrant (retrosoesophageal) RSA (A-RSA, asterisk). (K) A-RSA combined with cervical aortic arch (cAoA, black arrowhead). (L) A-RSA only (asterisk). LS, left side; RS, right side; AS, aortic sac; DoA, dorsal aorta; rcc, right common carotid; rsa, right subclavian artery; lcc, left common carotid; lsa, left subclavian artery; Ao, aorta.

Gbx2 expression is detected in the region where PAAs 3 to 6 are going to form (the bracketed domain in Fig. 1C,F) and is ultimately restricted to the P.endo (Fig. 1I,J) (Zhang et al., 2005).

We next examined *Gbx2* expression in *Tbx1*$^{-/-}$ embryos at E8.5 and found that it was lost from both the PSE and the P.endo (Fig. 1G,H), but was maintained at the midbrain/hindbrain junction and in the tail bud region (Fig. 1G). By contrast, when we examined *Gbx2* expression in *Tbx1* PSE conditional mutants (*Tbx1*$^{flox/flox}$;*AP2α*$^{Cre/+}$, referred to here as *Tbx1-PSE*) (*AP2α* is also known as *Tcfap2a* – Mouse Genome Informatics), we found that it was lost in the PSE, whereas it was maintained in the P.endo (compare Fig. 1M with 1N and Fig. 1B with 1O). Therefore, decreased *Gbx2* expression is more likely to be due to gene downregulation than to a lack of development/survival of *Gbx2*-expressing cells in the PSE. At later stages, *Tbx1*$^{-/-}$ mutants displayed severe hypoplasia of the pharynx, lacked the caudal PAs and lost *Gbx2*-expressing tissues (Fig. 1K,L).

Overall, our results showed that at the time of PAA specification, *Gbx2* expression domains, which consist of the PSE and P.endo, are dependent on *Tbx1* activity.

Gbx2 and *Tbx1* interact in vivo in the development of the fourth PAA

The gene expression data presented above suggest that *Gbx2* might interact with *Tbx1* in the PSE and/or P.endo. To test this hypothesis, we crossed *Tbx1*$^{+/-}$ with *Gbx2*$^{+/-}$ mice and analysed the PAA phenotype of the progeny at E10.5 and at E15.5 by ink injection. At E10.5, we scored a total of 42 embryos and found a variety of defects, as described in Fig. 2A-H and Table 1. In our mixed genetic background (see Materials and methods), we found that 5 out of 11 *Tbx1*$^{+/-}$;*Gbx2*$^{+/+}$ embryos (45.5%) were abnormal (Table 1). Under these conditions, dosage reduction to one copy of the *Gbx2* allele strongly increased the penetrance and severity of the fourth PAA phenotype: 12 out of 14 *Tbx1*$^{+/-}$;*Gbx2*$^{+/-}$ embryos (85.7%) were abnormal, which is significantly higher than that found for *Tbx1*$^{+/-}$;*Gbx2*$^{+/+}$ embryos (P=0.04). Furthermore, whereas the type

Table 1. Pharyngeal arch artery defects in compound heterozygotes at E10.5 and E15.5

			Fourth PAA defects scored by ink injection at E10.5			
					Bilateral defects	
Genotype	*n*	Abn (%)	Unilateral defect	Bilateral defect	Th-P/NP	NP/NP
Tbx1$^{+/+}$;*Gbx2*$^{+/+}$	6	0	0	0	0	0
Tbx1$^{+/+}$;*Gbx2*$^{+/-}$	11	0	0	0	0	0
Tbx1$^{+/-}$;*Gbx2*$^{+/+}$	11	5 (46)	3	2	1	1
Tbx1$^{+/-}$;*Gbx2*$^{+/-}$	**14**	**12 (86)***	**2**	**10**	**3**	**7**
			Aortic arch patterning defects scored at E15.5			
Genotype	*n*	Abn (%)	A-RSA	A-RSA and cAoA	IAA-B	IAA-B and A-RSA
Tbx1$^{+/+}$;*Gbx2*$^{+/+}$	29	0	0	0	0	0
Tbx1$^{+/+}$;*Gbx2*$^{+/-}$	16	0	0	0	0	0
Tbx1$^{+/-}$;*Gbx2*$^{+/+}$	19	5 (26)	2	0	0	2
Tbx1$^{+/-}$;*Gbx2*$^{+/-}$	22	13 (59)*	5	2	1	5

n, number of embryos scored; Abn, abnormal; Th-P/NP, one artery is thin and the other is not patent to ink; NP/NP, neither artery is patent to ink; A-RSA, aberrant origin of the right subclavian artery; cAoA, cervical aortic arch; IAA-B, interrupted aortic arch type B.
*P=0.04;**P=0.035.

of defects found in *Tbx1*$^{+/-}$;*Gbx2*$^{+/+}$ embryos mostly affected the fourth PAA on one side only (3 out of 5 presented unilateral defects, Table 1), those found in *Tbx1*$^{+/-}$;*Gbx2*$^{+/-}$ embryos were much more severe, with 10 out of 12 affected on both sides, and 7 out of 10 harbouring no fourth PAA (NP/NP) (Fig. 2A-H; Table 1). The third and sixth PAAs were normal in all genotypes.

Similar to our findings in E10.5 embryos, the penetrance of arch defects was significantly higher in *Tbx1*$^{+/-}$;*Gbx2*$^{+/-}$ mutants (59%, n=22) than in *Tbx1*$^{+/-}$;*Gbx2*$^{+/+}$ embryos at E15.5 (26%, n=19) (see Table 1; Fig. 2I-L). Defects included an aberrant origin of the right subclavian artery (A-RSA), either alone or combined with interruption of the aortic arch type B (IAA-B) (Fig. 2J-L). Overall, our results showed that *Tbx1* and *Gbx2* interact genetically during fourth PAA development.

Gbx2 is a downstream effector of Tbx1 in the PSE during fourth PAA development

So far, our results suggest that Gbx2 might mediate a number of important Tbx1 functions during PAA morphogenesis. However, tissues expressing *Gbx2* and *Tbx1* interact closely during pharyngeal development, raising the issue of whether Gbx2 might be required in one or more domains, possibly extending beyond *Tbx1*-expressing tissues, to contribute to the development of the PAAs. We used lineage-specific and tissue-specific gene ablation experiments to address these points.

Ablation of *Gbx2* in *Tbx1*-expressing domains causes PAA defects

In order to test whether cells expressing both *Tbx1* and *Gbx2* are responsible for the fourth PAA phenotype, we performed lineage-specific gene ablation using a *Tbx1-Cre* transgenic mouse line combined with *Gbx2*$^{+/-}$ and *Gbx2*$^{flox/+}$ alleles (see Materials and methods). The *Tbx1-Cre* transgenic mouse has been used successfully to investigate *Fgf8* functions downstream of *Tbx1* (Brown et al., 2004).

Tbx1$^{Cre/+}$;*Gbx2*$^{flox/-}$ embryos were collected at E10.5 and fourth PAA formation was evaluated by ink injection (Table 2). Twenty-seven percent of conditional mutant embryos displayed an abnormal fourth PAA on one or both sides of the embryo; no other defects were found for any other genotypes produced in this cross. The low penetrance of the fourth PAA phenotype found in *Gbx2* conditional mutants did not recapitulate the percentage of defects found in *Gbx2*$^{-/-}$ embryos (50%, Table 2). This discrepancy is likely to be due to the low efficiency of *Tbx1-Cre*-driven transgene recombination in epithelial tissues at the time of fourth PAA specification (see Fig. S1 in the supplementary material), as previously reported (Macatee et al., 2003). Nevertheless, these results clearly demonstrate that deletion of *Gbx2* in *Tbx1*-expressing cells is sufficient to generate a fourth PAA phenotype, in agreement with a model in which *Tbx1* regulates *Gbx2* in a cell-autonomous manner.

We also noted that the genetic background affected the incidence of defects found in *Gbx2*$^{-/-}$ embryos, which reached 50% on a mixed background (Table 2) as compared with 100% on a C57Bl/6 background (Byrd and Meyers, 2005). This phenotypic variability was also found in different genetic backgrounds for the same *Tbx1* deletion (Taddei et al., 2001). For this reason, and also because the fourth PAA defect recovers partially over time (Lindsay and Baldini, 2001), we decided to focus on PAA formation scored at E10.5 and not to assay PAA remodelling at later stages.

Ablation of *Gbx2* in the PSE is sufficient to recapitulate fourth PAA defects exhibited by *Gbx2*$^{-/-}$ embryos

In order to abrogate *Gbx2* activity specifically in the PSE during embryonic development, we used an *AP2α-Cre* deleter mouse line, which has been successfully used to define *Fgf8* functions in that

Table 2. Fourth pharyngeal arch artery defects in *Gbx2* mutants at E10.5

Genotype	*n*	Abn (%)	Unilateral defects	Bilateral defects
Gbx2$^{+/+}$	21	0	0	0
Gbx2$^{+/-}$	33	0	0	0
Gbx2$^{-/-}$	12	6(50)*	6†	0
Gbx2$^{flox/+}$	10	0	0	0
Gbx2$^{flox/+}$;*Tbx1*$^{Cre/+}$ and *Gbx2*$^{flox/-}$	24	0	0	0
Gbx2$^{flox/-}$;*Tbx1*$^{Cre/+}$	11	3(27)**	2‡	1§
Gbx2$^{flox/+}$	12	0	0	0
Gbx2$^{flox/+}$;*AP2α*$^{Cre/+}$ and *Gbx2*$^{flox/-}$	31	0	0	0
Gbx2$^{flox/-}$;*AP2α*$^{Cre/+}$	15	7(47)***	5¶	2††

†Three embryos had a fourth PAA that was non-patent (NP) to ink on one side; three had a fourth PAA that was thin and patent to ink (Th-P) on one side.
‡Embryos had a fourth PAA NP to ink on one side only.
§A single embryo had fourth PAA NP to ink on both sides.
¶Four embryos had aberrant branching of fourth PAA on one side only; one had Th-P fourth PAA on one side.
††Both embryos had fourth PAA NP to ink on one side and aberrant branching on the other side; one embryo also had Th-P left sixth PAA.
n, number of embryos scored; Abn, abnormal.
*P≤0.01; **P=0.025; ***P≤0.01.

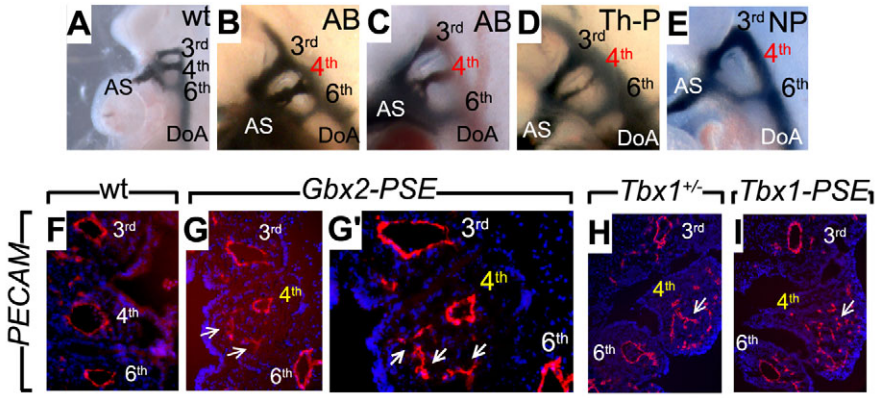

Fig. 3. *Gbx2-PSE* conditional mutants recapitulate fourth PAA abnormalities exhibited by *Gbx2*$^{-/-}$ mutants. (**A-E**) E10.5 ink-injected *Gbx2*$^{flox/-}$;*AP2α*$^{Cre/+}$ mouse embryos display aberrantly branched (AB) (B,C), Th-P (D) or NP (E) fourth PAAs as compared with wt embryos (A). (**F-I**) PECAM staining of a E10.5 wt embryo (F), Th-P *Gbx2-PSE* (G), NP *Tbx1*$^{+/-}$ (H) and NP *Tbx1-PSE* (*Tbx1*$^{flox/flox}$;*AP2α*$^{Cre/+}$) (I) mutant embryos. (G′) High-magnification view of G. White arrows indicate disorganised endothelial cells.

tissue (Macatee et al., 2003). Lineage-tracing analyses of the *AP2α-Cre* driver line detect Cre activity in the PSE as early as E8.5 (Macatee et al., 2003) (see Fig. S1 in the supplementary material), and also indicate labelling of pharyngeal NCCs (Macatee et al., 2003), a cell population that expresses neither *Gbx2*, *Tbx1* nor *Fgf8* (Fig. 1J, asterisk) (Bouillet et al., 1995; Chapman et al., 1996; Frank et al., 2002; Garg et al., 2001). Therefore, using the *AP2α-Cre* driver in our model corresponds to ablating *Gbx2* expression in the PSE at the onset of PAA formation.

We first analysed fourth PAA formation at E10.5 by performing ink injection on *Gbx2-PSE* conditional mutants. We found that the incidence of defects attributable to abnormal fourth PAA development was the same in *Gbx2*$^{-/-}$ and *Gbx2-PSE* embryos, with 47% of *Gbx2-PSE* embryos displaying abnormal fourth PAA as compared with 50% for *Gbx2*$^{-/-}$ (Fig. 3A-E; Table 2).

We next investigated PAA formation defects found in *Gbx2-PSE* mutants at the cellular level. A PECAM (Pecam1 – Mouse Genome Informatics) study of a thin-patent (Th-P) *Gbx2-PSE* conditional mutant at E10.5 showed that endothelial cells were present in the developing fourth PAA, but many failed to organise into tubes, as previously reported for *Gbx2*$^{-/-}$ mutants (Fig. 3G,G′) (Byrd and Meyers, 2005). In order to compare the *Gbx2*-type with the *Tbx1*-type PAA defects, we stained a non-patent (NP) *Tbx1*$^{+/-}$ embryo and a NP *Tbx1-PSE* (*AP2α*$^{Cre/+}$;*Tbx1*$^{flox/flox}$) conditional mutant embryo for PECAM and observed the same endothelial cell organisation defects at E10.5 (Fig. 3H,I). We therefore conclude that ablation of *Gbx2* in the PSE is sufficient to recapitulate the fourth PAA defects found in *Gbx2*$^{-/-}$ embryos.

Ablation of *Gbx2* in the PSE causes cNCC migration defects leading to fourth PAA defects

In order to investigate the origin of the fourth PAA abnormalities, we first tested whether *Gbx2-PSE* mutants recapitulate the cNCC patterning defects found in *Gbx2*$^{-/-}$ embryos (Meyers et al., 1998). Analysis of *Sox10* expression at E10.5, which marks migrating NCCs (Kuhlbrodt et al., 1998), revealed migration defects in 50% of embryos (*n*=8) (Fig. 4B). Whereas two discrete streams of cells were observed in wt embryos, these streams were partially or

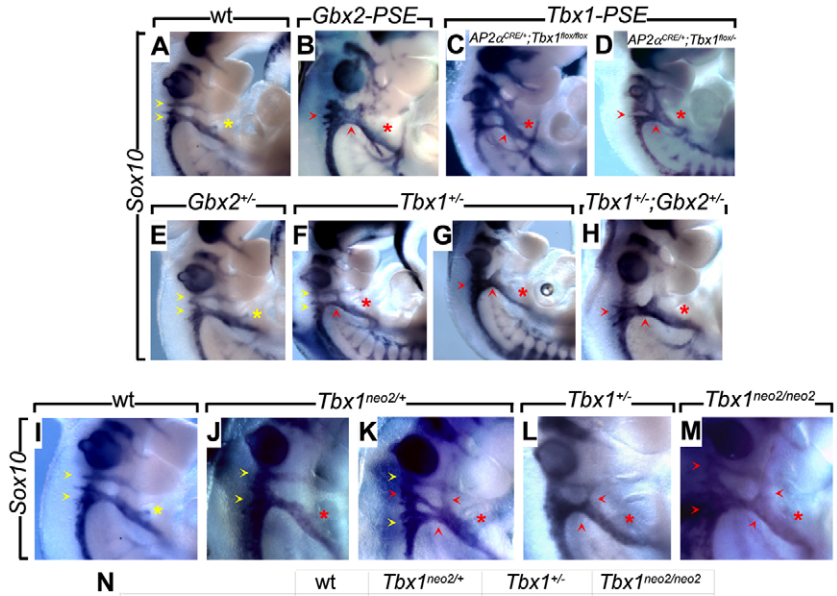

N

	wt	*Tbx1*$^{neo2/+}$	*Tbx1*$^{+/-}$	*Tbx1*$^{neo2/neo2}$
Tbx1 mRNA dosage	100%	70.1%[a]	50%[a]	34%[a]
cNCC migration defects	0%	40%[b]	100%[b]	100%[b]
4th PAA defects	0%	33%[b]	80%[a]	100%[a]

Fig. 4. Fourth PAA defects exhibited by *Gbx2-PSE*, *Tbx1-PSE* and *Tbx1*$^{+/-}$ embryos correlate with aberrant cNCC migration patterns. (**A-M**) *Sox10* ISH on E10.5 mouse embryos of the genotypes indicated. Yellow and red arrows indicate normal and abnormal post-otic streams of migrating cNCCs, respectively. cNCCs entering the fourth PA are marked by a yellow asterisk when normal (A,E,I) and by a red asterisk when absent (B-D,F-H,J-M). (**N**) Correlation of cNCC migration defects found in different *Tbx1* hypomorphic mutants on a C57Bl/6 background (I-M) with resulting fourth PAA defects at E10.5. [a](Zhang and Baldini, 2008); [b]this study.

completely fused in *Gbx2-PSE* embryos [compare yellow (normal) with red (abnormal) arrows in Fig. 4A,B]. This aberrant migration pattern was accompanied by a loss of cNCCs entering the fourth PA specifically [compare yellow (normal) with red (abnormal) asterisks in Fig. 4A,B]. In addition, we found that two types of *Tbx1-PSE* conditional mutants ($AP2\alpha^{Cre/+};Tbx1^{flox/flox}$ and $AP2\alpha^{Cre/+};Tbx1^{flox/-}$) suffered from similar cNCC migration defects (Fig. 4C,D). Furthermore, cNCC migration defects were more severe in $Tbx1^{+/-};Gbx2^{+/-}$ embryos as compared with *Tbx1* or *Gbx2* heterozygous embryos (Fig. 4E-H), in agreement with a genetic interaction between *Gbx2* and *Tbx1* during fourth PAA development (Fig. 2; Table 1).

In addition to the cNCC migration phenotype observed in all *Gbx2* and *Tbx1* mutants, the decreased number of cNCCs entering the fourth PA could result from a lack of survival of these cells within this specific PA, as previously reported (Arnold et al., 2006; Macatee et al., 2003). In order to test this, we performed dual fluorescence staining at E10.5 using p75 (Ngfr – Mouse Genome Informatics) antibody and Lysotracker reagent, which mark NCCs (Rao and Anderson, 1997) and areas containing apoptotic cells, respectively (Barbosky et al., 2006). In wt or $Gbx2^{+/-}$ embryos, cNCC patterning occurred normally and cNCCs migrated into the caudal fourth PA, which was filled with green, p75-positive cells (Fig. 5Aa,Ad). In *Gbx2-PSE* embryos, cNCC migration was abnormal (yellow arrows in Fig. 5Ba) and the number of p75-positive cells within the fourth PA was substantially decreased (yellow asterisks in Fig. 5Ba,Bd). This aberrant migration was not accompanied by an increase in the number of apoptotic cells in the region caudal to the otocyst along the migratory path (compare the Lysotracker reagent pattern in Fig. 5Ab and Bb), none of these cells being p75 positive (note the absence of double-labelled cells in Fig. 5Ac and 5Bc). Similar results were observed at E9.5 (data not shown). Furthermore, we did not detect any increase in apoptosis in the PSE, P.endo or mesodermal tissues within the fourth PA (Fig. 5Ad,Bd). Similar results were obtained with $Tbx1^{+/-}$ and $Gbx2^{+/-};Tbx1^{+/-}$ embryos (Fig. 5C,D). In all mutants, cNCC deficiency was accompanied by a missing fourth PAA (Fig. 5Bd,Cd,Dd). We therefore conclude that cNCC deficiency at the level of the fourth PA does not originate from a lack of survival signals triggered by the PSE, but rather from an incorrect migration signal that misguides these cells from their intended destination.

Surprisingly, we found that 100% of $Tbx1^{+/-}$ embryos (n=6) displayed cNCC migration abnormalities (Fig. 4F,G; Fig. 5C) in a c57Bl/6 background, a defect that has not been documented previously and is contrary to studies suggesting that cNCC migration occurs normally in $Tbx1^{+/-}$ embryos (Kochilas et al., 2002; Lindsay and Baldini, 2001). Our analysis shows that although the number of cNCCs migrating into the caudal PAs is not affected (Fig. 4F,G; Fig. 5C) (Kochilas et al., 2002), their migration paths are disrupted, which in turn leads to a cNCC deficiency at the level of the fourth PA. To elaborate on these findings, we investigated how this cNCC response varied with *Tbx1* dosage. We examined cNCC migration defects in a *Tbx1* hypomorphic series (see Materials and methods) and compared this with the incidence of fourth PAA defects (Zhang and Baldini, 2008). We found that progressive diminution of *Tbx1* mRNA levels in vivo, which is associated with increased penetrance of the fourth PAA phenotype (Zhang and Baldini, 2008), correlated with an increased incidence of cNCC migration defects (Fig. 4I-N). Overall, our data present for the first time a non-cell-autonomous function for *Tbx1* in cNCC migration and correlate fourth PAA deficiency with cNCC migration defects.

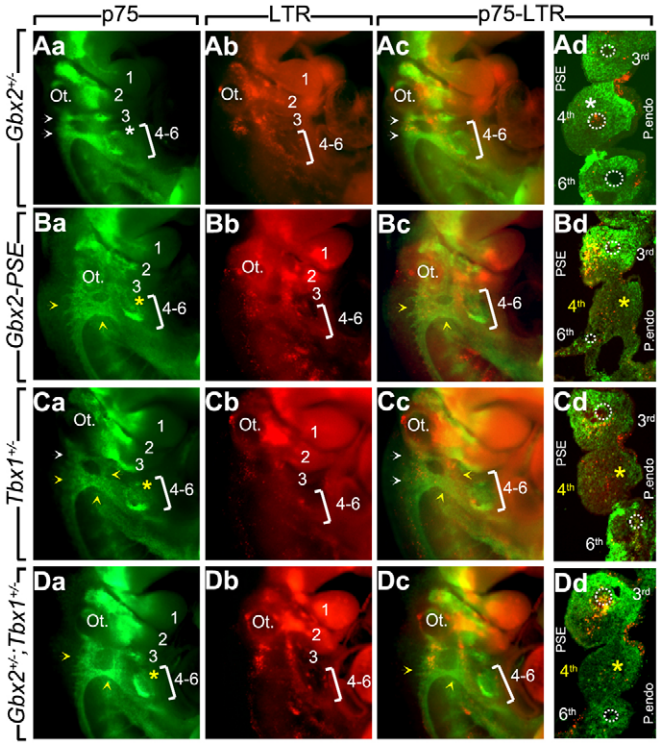

Fig. 5. cNCC deficiency at the level of the fourth PA is not caused by increased cell death. (**Aa-Dd**) Double fluorescence staining of cNCCs (p75) and apoptotic cells (Lysotracker reagent) on E10.5 mouse embryos of the genotypes indicated. White and yellow arrows indicate normal (Aa-Ad) and abnormal (Ba-Dd) post-otic streams of migrating cNCCs, respectively. cNCCs entering the fourth PA are marked by a white asterisk when normal and by a yellow asterisk when abnormal. Reduced numbers of cNCCs reaching the fourth PA were observed in all mutant genotypes (Ba-Dd). Ot, otic vesicle.

In summary, our data suggest that loss of *Tbx1* and *Gbx2* in the PSE results in fourth PAA abnormalities associated with cNCC deficiency in the fourth PA. Our data also demonstrate that this striking reduction of cNCCs in the fourth PAA is linked to a severe diversion of cNCC routes, rather than to any increased apoptosis of these cells. Finally, we propose a central function for cNCCs in arterial development and endothelial cell organisation at E10.5, prior to their differentiation into smooth muscle cells at E11/E11.5 (Bergwerff et al., 1999; Byrd and Meyers, 2005).

Ectoderm-derived Gbx2 acts independently of Fgf8 in the development of the fourth PAA

Fgf8 is expressed in the PSE (Crossley and Martin, 1995), interacts genetically with *Tbx1* in the development of the fourth PAA (Vitelli et al., 2002b) and specific deletion of *Fgf8* in the PSE causes fourth PAA defects (Macatee et al., 2003). It is therefore possible that Gbx2 performs some of the developmental functions of Fgf8 in this tissue, as previously suggested (Byrd and Meyers, 2005; Liu et al., 1999). In order to test this, we performed whole-mount in situ hybridisation for *Gbx2* on $Fgf8^{neo/\Delta 2,3}$ hypomorphic embryos at E8.5 and E9.5. No change in *Gbx2* expression in the PSE was detected (see Fig. S2 in the supplementary material). As a result, we conclude that *Gbx2* acts downstream of *Tbx1*, but independently of *Fgf8*, in the development of the fourth PAA.

Gbx2 affects a Slit/Robo signalling pathway implicated in cNCC migration

The Slit/Robo signalling pathway is involved in trunk neural crest migration (Jia et al., 2005) and is also implicated in *Drosophila* cNCC-like motility and assembly into the OFT (Zmojdzian et al., 2008). The gene encoding the secreted protein Slit2 was identified as a potential downstream target of Tbx1 in a new series of gene expression arrays, in which *Tbx1*-expressing cells, isolated directly from embryos, were submitted to transcriptome analysis (K.L.V.B. and P.J.S., unpublished data; see Materials and methods). *Slit2* was found to be downregulated in $Tbx1^{+/-};Df1^{+/-}$ cells [effectively $Tbx1^{-/-}$ (Lindsay et al., 1999)] as compared with $Tbx1^{+/-}$ cells [to 0.529±0.125 (mean±s.d.), $P<0.01$]. Therefore, we investigated elements of this pathway in wt and mutant embryos at the time of fourth PAA development by in situ hybridisation (Figs 6 and 7).

At E8.75, *Slit2* was detected in two major ectodermal regions covering both sides of the otic vesicle (Fig. 6A). *Slit2* was strongly expressed in the PSE, whereas it was barely detectable in the P.endo (Fig. 6B), a pattern which resembles that of *Gbx2* (Fig. 1B). In the PSE, Slit2 and Tbx1 colocalise at the time of PAA formation (Fig. 6E-G). Additionally, *Slit2* was detected in the floorplate of the neural tube and in the notochord (Fig. 6B). At E9.25, *Slit2* expression is robustly detected in the pharyngeal pouches (Fig. 6C) (Yuan et al., 1999) and was increased in the P.endo by E9.5 (Fig. 6D). Conversely, *Slit2* expression in the PSE was not longer detected at that stage (Fig. 6D). We also noted a potential Slit ligand redundancy as both *Slit1* and *Slit3* were expressed in the PSE at the time of PAA formation and in overlapping domains with *Slit2* (see Fig. S3 in the supplementary material).

Slit proteins mediate their effects through the Robo family of receptors, which consists of four members (Robo1-4). Slit2 can bind to all four Robo receptors (Brose et al., 1999; Camurri et al., 2005; Park et al., 2003), with *Robo4* expressed exclusively in the vascular endothelium (Park et al., 2003). When examining *Robo1-3* expression at the time of cNCC migration, we found that *Robo1* had the most relevant pattern of expression (Fig. 6H-K), although *Robo2* and *Robo3* were expressed in overlapping regions with *Robo1* (data not shown). *Robo1* was first detected in the neural tube at E8.5 (Fig. 6H) and labelled streams of migrating NCCs in the vagal and trunk regions of E9.5 embryos (Fig. 6I,J). *Robo1*-positive cNCC streams were observed as early as E9.0 (data not shown) and migrated through PAAs 4-6, which exhibited strong *Robo1* labelling at E11 (Fig. 6K). When comparing *Robo1* expression with two other NCC markers at E9.5, we found that the *Robo1*-positive stream of cells corresponded to that detected by *Sox10* or Hnk1 (B3gat1 – Mouse Genome Informatics) labelling (Fig. 6L-N,L′-N′). As Robo1 is also expressed in the dermomyotome (Sundaresan et al., 2004), we performed a double immunofluorescence on E9.5 wt embryos, which confirmed Robo1 colocalisation with AP2α-positive migrating NCCs (Mitchell et al., 1991) (Fig. 6O-Q′).

We next investigated the expression of Slit/Robo pathway components in *Gbx2* and *Tbx1* mutants as a possible mechanism contributing to aberrant cNCC migration (Fig. 7).

At E8.75, the ectodermal expression of *Slit2* was strongly downregulated in the post-otic region in $Gbx2^{-/-}$ embryos, whereas the pre-otic region of *Slit2* expression appeared unaffected (Fig. 7A,B). The same results were obtained in *Gbx2-PSE* and *Tbx1-PSE* ($AP2\alpha^{Cre/+};Tbx1^{flox/-}$) embryos and confirmed downregulation of *Slit2* specifically in the PSE (Fig. 7D,I). *Slit2* expression was also downregulated in $Tbx1^{-/-}$ embryos in both regions spanning either side of the otic vesicle (Fig. 7E,F) and in the post-otic region of $Tbx1^{+/-};Gbx2^{+/-}$ embryos (Fig. 7H). *Slit2* downregulation was more severe in *Tbx1-PSE* and $Tbx1^{-/-}$ mutants than in *Gbx2-PSE* and $Gbx2^{-/-}$ mutants (Fig. 7B,D,F,I), suggesting that *Tbx1* might also regulate *Slit2* expression independently of *Gbx2*.

When examining *Robo1* expression in E9.5 $Gbx2^{-/-}$ embryos, we found that the number of *Robo1*-positive cNCCs migrating towards caudal PAs was reduced (compare yellow arrow in Fig. 7J with black arrow in Fig. 6M). Similarly, *Robo1*-positive cells appeared less abundant in E10.5 *Gbx2-PSE* embryos (Fig. 7L) than in wt embryos (black bracketed region in Fig. 7K). We also observed fewer *Robo1*-positive cells at the level of the caudal arches, and the overall *Robo1* expression domain appeared disorganised (yellow arrows in Fig. 7L). A similar decrease in *Robo1*-expressing

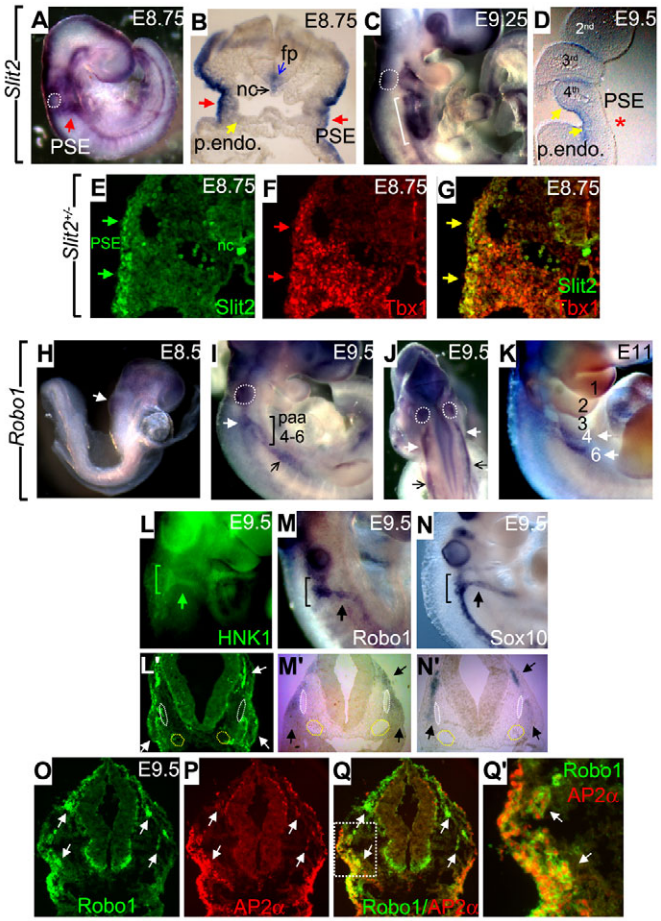

Fig. 6. The Slit/Robo pathway signals to cNCCs at the time of fourth PAA specification. (**A-D**) ISH for *Slit2* labelling the PSE (red arrows) or not (red asterisks in D), and the P.endo (yellow arrow) in the pharyngeal pouches (bracketed region in C). (**E-G**) Double immunofluoresence on E9.0 $Slit2^{+/-}$ embryos with anti-GFP (E) labelling of Slit2-expressing cells and with anti-Tbx1 (F) antibodies. (**H-K**) ISH for *Robo1* labelling of migrating cardiac and trunk NCCs at E9.5 (white and black arrows, respectively). (**L-N′**) *Robo1* expression (M,M′) compared with two NCC markers, *Sox10* (N,N′) and Hnk1 (L,L′). Dotted circles correspond to the otic vesicle in A,C,I,J; white and yellow dotted lines correspond to the dorsal aorta and the cardinal vein, respectively, in L′-N′. (**O-Q′**) Double immunofluoresence on E9.5 wt embryos with anti-Robo1 (O) and anti-AP2α (P) antibodies. (Q′) High-magnification view of the boxed area in Q. White arrows indicate migrating NCCs. nc, notochord; fp, floorplate of the neural tube.

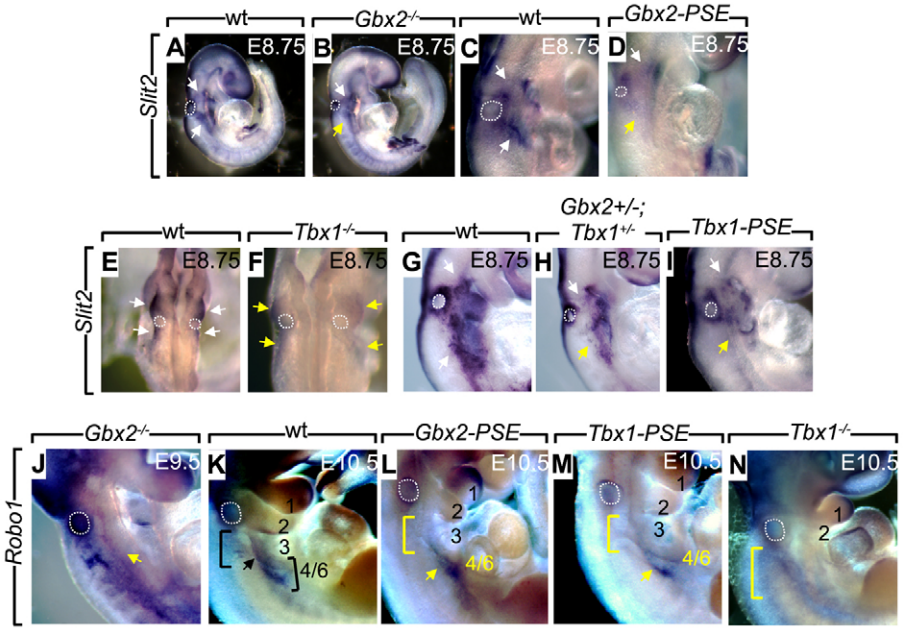

Fig. 7. The Slit/Robo pathway is altered in the pharyngeal region of *Tbx1* and *Gbx2* mutant embryos. (**A-I**) ISH for *Slit2* in wt (A,C,E,G) and mutant (B,D,F,H,I) E8.75 mouse embryos. Yellow and white arrows indicate downregulation or normal expression of *Slit2*, respectively. (**J-N**) A decreased number of migrating *Robo1*-positive cNCCs was detected in E9.5 $Gbx2^{-/-}$ embryos (J) and in the caudal PAs of E10.5 *Gbx2-PSE*, *Tbx1-PSE* ($Tbx1^{flox/-}$;$AP2\alpha^{Cre/+}$) and $Tbx1^{-/-}$ embryos (yellow arrow and bracketed region in L,M,N) as compared with wt (K).

domains was observed in *Tbx1-PSE* conditional mutants ($AP2\alpha^{Cre/+}$;$Tbx1^{flox/-}$) and $Tbx1^{-/-}$ mutants (Fig. 7M,N). These findings suggest that in response to a lower dosage of *Slit2* in the PSE, *Robo1*-expressing domains are affected and *Robo1* expression appears downregulated in the cNCC lineage of *Gbx2* and *Tbx1* mutants. These results are consistent with examples of the tight regulation of Robo expression in other systems (Andrews et al., 2008; Plachez et al., 2008). In conclusion, our data provide the first evidence for a Slit/Robo-mediated signalling pathway implicated in cNCC migration during PAA formation.

DISCUSSION

In this study, we have described a new function for the T-box transcription factor Tbx1 in controlling cell migration during PAA formation. We found that within the PSE, Tbx1 regulates the expression of the homeobox gene *Gbx2*, which in turn directs accurate cNCC navigation to caudal PAs. We investigated two potential mechanisms of action and found that this control is Fgf8-independent but imparts the activation of the Slit/Robo signalling pathway.

Gbx2 interacts with *Tbx1* and mediates essential *Tbx1* functions during fourth PAA formation

A number of genes, including *Fgf8*, *Crk1* (*Mapk14*) and $Vegf^{164}$ (*Vegfa*), interact genetically with *Tbx1* during fourth PAA development (Guris et al., 2006; Stalmans et al., 2003; Vitelli et al., 2002b). However, no potential downstream effectors of Tbx1 during PAA development have been reported so far.

Our cross-breeding experiments showed that *Gbx2* interacts genetically with *Tbx1*, causing significant enhancement of the fourth PAA *Tbx1* haploinsufficiency phenotype at both E10.5 and E15.5. Recovery from fourth PAA defects has previously been observed in *Df1/+* mutants (Lindsay and Baldini, 2001) and did not appear to be affected by mutation of *Gbx2*, as a similar proportion of embryos overcame the early defect in $Tbx1^{+/-}$ mutants and $Tbx1^{+/-}$;$Gbx2^{+/-}$ double mutants by E15.5. These results suggested that the interaction with *Tbx1* contributes to the primary defect, i.e. early in fourth PAA morphogenesis, rather than at the subsequent remodelling stage.

We generated a series of conditional mutants to test a putative role for Gbx2 downstream of Tbx1 in fourth PAA development. We employed a *Tbx1-Cre* line to show that Gbx2 is required in Tbx1-expressing cells and validated a model in which Gbx2 is a downstream effector of Tbx1 during fourth PAA development. Although three consensus T-box-binding sequences have been described within the first 5 kb of the *Gbx2* promoter (Ivins et al., 2005), we have so far failed to identify any transactivation of reporters coupled to promoter fragments containing these elements (data not shown). The molecular mechanism underlying differential expression of *Gbx2* in *Tbx1* mutants remains to be determined.

Tissue-specific expression of *Tbx1* in the SHF mesoderm is required for proper OFT development (Zhang et al., 2006) and some OFT-related defects have been reported to occur at a low frequency in $Gbx2^{-/-}$ mutants (Byrd and Meyers, 2005). Although it is unlikely that Gbx2 mediates the effects of Tbx1 in OFT development, as *Gbx2* expression was not detected in the SHF, it is still possible that Tbx1 and Gbx2 could regulate adjacent pathways that control different aspects of OFT morphogenesis. Nevertheless, no cardiac defects were observed, neither in $Tbx1^{+/-}$;$Gbx2^{+/-}$ embryos (apart from a single ventricular septal defect, data not shown), nor in *Gbx2-PSE* (n=4) or *Gbx2;Tbx1-Cre* (n=23) mutant embryos. In addition, no thymic defects were noted. Thus, the phenotype-enhancing effect of *Gbx2* appeared to be restricted to fourth PAA defects.

The PSE acts as a signalling centre for migrating cNCCs

Our work confirmed the crucial role played by the PSE during PAA development. Since the same incidence of defects was found in *Gbx2-PSE* embryos as in $Gbx2^{-/-}$ embryos, we concluded that *Gbx2* is required in the PSE to pattern the fourth PAAs. These findings are in agreement with Gbx2 being a downstream effector of Tbx1 in the ectoderm, as defective fourth PAA development has also been reported in *Tbx1-PSE* conditional mutants (E.A.I., unpublished data). As *Gbx2* expression was also downregulated in the pharyngeal endoderm of $Tbx1^{-/-}$ embryos, it remains possible that this tissue plays a synergistic role in conjunction with the PSE in patterning fourth PAAs. Nevertheless, this role is likely to be subtle,

as *Gbx2-PSE* mutants recapitulate cNCC migration anomalies as well as the endothelial cell organisation defects and fourth PAA abnormalities found in *Gbx2*$^{-/-}$ embryos.

We found that two genes, *Gbx2* and *Slit2*, which are both implicated in the *Tbx1*-related fourth PAA phenotype (the role of *Slit2* is discussed below) are expressed in overlapping ectodermal domains with *Tbx1*. Notably, at ~E8.5, which corresponds to the time point at which *Tbx1* is required for fourth PAA patterning (Xu et al., 2005), *Gbx2* and *Slit2* displayed very strong expression in the PSE compared with the P.endo, and this expression was not maintained later in development. A similar transient ectodermal expression pattern has previously been described for *Tbx1* (Zhang et al., 2005). We speculate that this tight spatiotemporal control of gene expression is required for correct patterning of cNCCs. Indeed, cNCCs emigrate from the neural tube at the 7-9 somites stage in the mouse embryo (Chan et al., 2004; Trainor, 2005). Therefore, the timing of *Tbx1*, *Gbx2* and *Slit2* expression, accompanied by the position of the PSE, immediately juxtaposed to cNCCs as they start to migrate, is likely to be instructive. It would not be surprising to find that other genes expressed in the PSE also regulate cNCC function in relation to cardiovascular development, as is already known to be the case for *Fgf8* (Crossley and Martin, 1995; Macatee et al., 2003).

Tbx1 directs cNCC migration by controlling *Gbx2* expression

The best-characterised functions of Tbx1 during pharyngeal and heart development are its cell-autonomous effects on cell proliferation, cell fate decision and progenitor cell expansion (Xu et al., 2004; Xu et al., 2007; Zhang et al., 2005; Zhang et al., 2006). Little is known about the non-cell-autonomous role of Tbx1 in cNCC development.

Our study describes a new function for Tbx1 in regulating cNCC migration during PAA development and constitutes the second set of evidence that Tbx1 plays a role in cNCC development. Previously, histological analysis of the fourth PAAs in *Df1*/+ and *Lgdel*/+ embryos, two chromosome deletion mouse models for DiGeorge syndrome reducing *Tbx1* to hemizygosity (Lindsay et al., 1999; Merscher et al., 2001), revealed a role for Tbx1 in cNCC differentiation into vascular smooth muscle (Kochilas et al., 2002; Lindsay and Baldini, 2001) as a possible explanation of the *Tbx1* haploinsufficiency phenotype. Nevertheless, additional defective signalling pathways are likely to be involved in the fourth PAA phenotype at E10.5 as cNCC differentiation into vascular smooth muscle is not stably detected at the level of the fourth PAA until E11.5 (Bergwerff et al., 1999; Byrd and Meyers, 2005). Our work demonstrated that the fourth PAA phenotype originates from a cNCC deficiency at the level of the fourth PA in both *Gbx2* and *Tbx1* mutants, highlighting a central function for the cNCCs in arterial development prior to their differentiation into smooth muscle cells.

Evidence for a role for *Tbx1* in regulating cNCC migration has been obtained previously. In *Lgdel*/+ mice, the number of cNCCs reaching the cardiac cushions of the OFT was affected (Kochilas et al., 2002), and in *Tbx1*$^{-/-}$ embryos, post-otic cranial nerves IX and X, which derive in part from cNCCs and follow similar migratory streams as they develop, were abnormally fused in their distal part (Vitelli et al., 2002a). We demonstrated that Tbx1 acts on cNCC migration by controlling the expression of *Gbx2*, a gene implicated exclusively in the migratory aspect of cNCCs (Byrd and Meyers, 2005). We provided evidence that migrating streams of cNCCs are disorganised in *Gbx2-PSE*, *Tbx1*$^{+/-}$ and *Tbx1-PSE* mutant embryos by analysing three markers of migrating cNCCs: *Sox10*, p75 and *Robo1*. This dysregulation of migratory path-finding results in a reduced number of these cells reaching the fourth PAs and is associated with abnormal organisation of adjacent endothelial cells into tubes and, subsequently, with fourth PAA abnormalities.

Finally, our data have shown that the Tbx1/Gbx2 pathway acts independently of Fgf8 in the PSE during PAA development, which is in agreement with separate roles for Tbx1/Gbx2 and Fgf8 in controlling cNCC migration and survival, respectively (Macatee et al., 2003). Indeed, in *Tbx1* and *Gbx2* mutants, cNCCs do not apoptose within the fourth PA, but instead fail to reach this location because their migration paths have been diverted.

The Slit/Robo signalling pathway: a novel role in cNCC migration

cNCCs represent a transitional population between the cranial and the trunk crest region and share properties common to both cells (Suzuki and Kirby, 1997). It is therefore likely that signalling molecules implicated in cranial and trunk crest cell migration, such as Semaphorins, Ephrins and Slits, are also used by cNCCs to reach their targets. So far, very little is known about how cNCC migration is regulated, although one series of reports has implicated the Semaphorin family of secreted ligands (Brown et al., 2001; Feiner et al., 2001; Toyofuku et al., 2008).

We showed that *Slit2* is downregulated in the PSE of *Gbx2*$^{-/-}$, *Gbx2-PSE*, *Tbx1-PSE* and *Tbx1*$^{-/-}$ embryos at the time of fourth PAA development. We also showed that at least one member of the Roundabout family, *Robo1*, is expressed in the NCC lineage. These findings support a new role for *Tbx1* in regulating cNCC migration and indicate a possible pathway utilised by cNCCs to reach their targets during development. NCCs migrate in segmentally restricted streams, the boundaries of which are maintained by signalling molecules such as those of the Slit/Robo family (De Bellard et al., 2003). In *Gbx2*$^{-/-}$, *Gbx2-PSE*, *Tbx1-PSE* and *Tbx1*$^{-/-}$ embryos, fusion of cNCC streams suggests that the molecular basis of distinct path formation has been disrupted. Whether Slit/Robo signalling mediates repulsive or attractive signals to maintain separated streams during cNCC migration is currently under investigation. Interestingly, a recent study demonstrated that both repulsive and attractive signals provided by the Semaphorin/Plexin family are required for precise navigation of cNCCs (Toyofuku et al., 2008).

Robo4 is a specific marker of endothelial cells and activation of *Robo4* by *Slit2* stabilises the vascular network by inhibiting endothelial tube formation and permeability as well as vascular leak (Jones et al., 2008). In addition, Robo1 and Robo4 are involved in filopodia formation and endothelial cell motility (Sheldon et al., 2009). Notably, *Gbx2*$^{-/-}$*;Gbx2-PSE*, *Tbx1*$^{+/-}$ and *Tbx1-PSE* embryos displayed abnormally organised endothelial cells (Byrd and Meyers, 2005). Therefore, a non-cell-autonomous action of Tbx1 on fourth PAA development could act in two synergistic ways by controlling both cNCC migration/differentiation and endothelial cell organisation. Likewise, investigating the role of the Slit/Robo pathway in fourth PAA development will require careful analysis of multiple potential players.

Acknowledgements

We thank Antonio Baldini and Bernice Morrow for *Tbx1* mutant mice; Gail Martin for *Fgf8* mutant mice; Marc Tessier-Lavigne for *Slit2* mutant mice; Catherine Roberts for critical comments on the manuscript; Alex Joyner for the *Gbx2* probe; Quenten Schwarz and Christiana Ruhrberg for the *Sox10* probe and anti-p75 antibody; D. Ornitz for the *Slit2* probe; Uta Grieshammer and Gail Martin for *Robo1-3* probes; and Nicola Smart, Suzanne Rix and Paul Riley for immunofluorescence regents. The research was supported by the British Heart Foundation grant RG/05/013 and CardioGeNet European grant to P.J.S.,

Medical Research Council grant G0601104 to M.A.B., Welcome Trust programme grant 074549 to W.D.A., grant R01DE/HD12324 to J.F.M. and R01HD044157 to A.M.M. Deposited in PMC for release after 6 months.

Supplementary material

Supplementary material for this article is available at http://dev.biologists.org/cgi/content/full/136/18/3173/DC1

References

Andrews, W., Barber, M., Hernadez-Miranda, L. R., Xian, J., Rakic, S., Sundaresan, V., Rabbitts, T. H., Pannell, R., Rabbitts, P., Thompson, H. et al. (2008). The role of Slit-Robo signaling in the generation, migration and morphological differentiation of cortical interneurons. *Dev. Biol.* **313**, 648-658.

Arnold, J. S., Werling, U., Braunstein, E. M., Liao, J., Nowotschin, S., Edelmann, W., Hebert, J. M. and Morrow, B. E. (2006). Inactivation of Tbx1 in the pharyngeal endoderm results in 22q11DS malformations. *Development* **133**, 977-987.

Barbosky, L., Lawrence, D. K., Karunamuni, G., Wikenheiser, J. C., Doughman, Y. Q., Visconti, R. P., Burch, J. B. and Watanabe, M. (2006). Apoptosis in the developing mouse heart. *Dev. Dyn.* **235**, 2592-2602.

Bergwerff, M., DeRuiter, M. C., Hall, S., Poelmann, R. E. and Gittenberger-de Groot, A. C. (1999). Unique vascular morphology of the fourth aortic arches: possible implications for pathogenesis of type-B aortic arch interruption and anomalous right subclavian artery. *Cardiovasc. Res.* **44**, 185-196.

Bockman, D. E. and Kirby, M. L. (1984). Dependence of thymus development on derivatives of the neural crest. *Science* **223**, 498-500.

Bouillet, P., Chazaud, C., Oulad-Abdelghani, M., Dolle, P. and Chambon, P. (1995). Sequence and expression pattern of the Stra7 (Gbx-2) homeobox-containing gene induced by retinoic acid in P19 embryonal carcinoma cells. *Dev. Dyn.* **204**, 372-382.

Brose, K., Bland, K. S., Wang, K. H., Arnott, D., Henzel, W., Goodman, C. S., Tessier-Lavigne, M. and Kidd, T. (1999). Slit proteins bind Robo receptors and have an evolutionarily conserved role in repulsive axon guidance. *Cell* **96**, 795-806.

Brown, C. B., Feiner, L., Lu, M. M., Li, J., Ma, X., Webber, A. L., Jia, L., Raper, J. A. and Epstein, J. A. (2001). PlexinA2 and semaphorin signaling during cardiac neural crest development. *Development* **128**, 3071-3080.

Brown, C. B., Wenning, J. M., Lu, M. M., Epstein, D. J., Meyers, E. N. and Epstein, J. A. (2004). Cre-mediated excision of Fgf8 in the Tbx1 expression domain reveals a critical role for Fgf8 in cardiovascular development in the mouse. *Dev. Biol.* **267**, 190-202.

Byrd, N. A. and Meyers, E. N. (2005). Loss of Gbx2 results in neural crest cell patterning and pharyngeal arch artery defects in the mouse embryo. *Dev. Biol.* **284**, 233-245.

Camurri, L., Mambetisaeva, E., Davies, D., Parnavelas, J., Sundaresan, V. and Andrews, W. (2005). Evidence for the existence of two Robo3 isoforms with divergent biochemical properties. *Mol. Cell. Neurosci.* **30**, 485-493.

Chan, W. Y., Cheung, C. S., Yung, K. M. and Copp, A. J. (2004). Cardiac neural crest of the mouse embryo: axial level of origin, migratory pathway and cell autonomy of the splotch (Sp2H) mutant effect. *Development* **131**, 3367-3379.

Chapman, D. L., Garvey, N., Hancock, S., Alexiou, M., Agulnik, S. I., Gibson-Brown, J. J., Cebra-Thomas, J., Bollag, R. J., Silver, L. M. and Papaioannou, V. E. (1996). Expression of the T-box family genes, Tbx1-Tbx5, during early mouse development. *Dev. Dyn.* **206**, 379-390.

Crossley, P. H. and Martin, G. R. (1995). The mouse Fgf8 gene encodes a family of polypeptides and is expressed in regions that direct outgrowth and patterning in the developing embryo. *Development* **121**, 439-451.

De Bellard, M. E., Rao, Y. and Bronner-Fraser, M. (2003). Dual function of Slit2 in repulsion and enhanced migration of trunk, but not vagal, neural crest cells. *J. Cell Biol.* **162**, 269-279.

DeRuiter, M. C., Poelmann, R. E., Mentink, M. M., Vaniperen, L. and Gittenberger-de Groot, A. C. (1993). Early formation of the vascular system in quail embryos. *Anat. Rec.* **235**, 261-274.

Feiner, L., Webber, A. L., Brown, C. B., Lu, M. M., Jia, L., Feinstein, P., Mombaerts, P., Epstein, J. A. and Raper, J. A. (2001). Targeted disruption of semaphorin 3C leads to persistent truncus arteriosus and aortic arch interruption. *Development* **128**, 3061-3070.

Frank, D. U., Fotheringham, L. K., Brewer, J. A., Muglia, L. J., Tristani-Firouzi, M., Capecchi, M. R. and Moon, A. M. (2002). An Fgf8 mouse mutant phenocopies human 22q11 deletion syndrome. *Development* **129**, 4591-4603.

Garg, V., Yamagishi, C., Hu, T., Kathiriya, I. S., Yamagishi, H. and Srivastava, D. (2001). Tbx1, a DiGeorge Syndrome candidate gene, is regulated by sonic hedgehog during pharyngeal arch development. *Dev. Biol.* **235**, 62-73.

Guris, D. L., Duester, G., Papaioannou, V. E. and Imamoto, A. (2006). Dose-dependent interaction of Tbx1 and Crkl and locally aberrant RA signaling in a model of del22q11 syndrome. *Dev. Cell* **10**, 81-92.

High, F. A., Zhang, M., Proweller, A., Tu, L., Parmacek, M. S., Pear, W. S. and Epstein, J. A. (2007). An essential role for Notch in neural crest during cardiovascular development and smooth muscle differentiation. *J. Clin. Invest.* **117**, 353-363.

Hu, T., Yamagishi, H., Maeda, J., McAnally, J., Yamagishi, C. and Srivastava, D. (2004). Tbx1 regulates fibroblast growth factors in the anterior heart field through a reinforcing autoregulatory loop involving forkhead transcription factors. *Development* **131**, 5491-5502.

Ivins, S., Lammerts van Beuren, K., Roberts, C., James, C., Lindsay, E., Baldini, A., Ataliotis, P. and Scambler, P. J. (2005). Microarray analysis detects differentially expressed genes in the pharyngeal region of mice lacking Tbx1. *Dev. Biol.* **285**, 554-569.

Jerome, L. A. and Papaioannou, V. E. (2001). DiGeorge syndrome phenotype in mice mutant for the T-box gene, Tbx1. *Nat. Genet.* **27**, 286-291.

Jia, L., Cheng, L. and Raper, J. (2005). Slit/Robo signaling is necessary to confine early neural crest cells to the ventral migratory pathway in the trunk. *Dev. Biol.* **282**, 411-421.

Jiang, X., Rowitch, D. H., Soriano, P., McMahon, A. P. and Sucov, H. M. (2000). Fate of the mammalian cardiac neural crest. *Development* **127**, 1607-1616.

Jones, C. A., London, N. R., Chen, H., Park, K. W., Sauvaget, D., Stockton, R. A., Wythe, J. D., Suh, W., Larrieu-Lahargue, F., Mukouyama, Y. S. et al. (2008). Robo4 stabilizes the vascular network by inhibiting pathologic angiogenesis and endothelial hyperpermeability. *Nat. Med.* **14**, 448-453.

Kirby, M. L. and Waldo, K. L. (1995). Neural crest and cardiovascular patterning. *Circ. Res.* **77**, 211-215.

Kirby, M. L., Gale, T. F. and Stewart, D. E. (1983). Neural crest cells contribute to normal aorticopulmonary septation. *Science* **220**, 1059-1061.

Kirby, M. L., Turnage, K. L., 3rd and Hays, B. M. (1985). Characterization of conotruncal malformations following ablation of 'cardiac' neural crest. *Anat. Rec.* **213**, 87-93.

Kochilas, L., Merscher-Gomez, S., Lu, M. M., Potluri, V., Liao, J., Kucherlapati, R., Morrow, B. and Epstein, J. A. (2002). The role of neural crest during cardiac development in a mouse model of DiGeorge Syndrome. *Dev. Biol.* **251**, 157-166.

Kuhlbrodt, K., Herbarth, B., Sock, E., Hermans-Borgmeyer, I. and Wegner, M. (1998). Sox10, a novel transcriptional modulator in glial cells. *J. Neurosci.* **18**, 237-250.

Le Douarin, N. M. and Kalcheim, C. (1999). *The Neural Crest*, 2nd edn. Cambridge: Cambridge University Press.

Le Lievre, C. S. and Le Douarin, N. M. (1975). Mesenchymal derivatives of the neural crest: analysis of chimaeric quail and chick embryos. *J. Embryol. Exp. Morphol.* **34**, 125-154.

Li, J. Y. H., Lao, Z. and Joyner, A. L. (2002). Changing requirements for Gbx2 in development of the cerebellum and maintenance of the mid/hindbrain organizer. *Neuron* **36**, 31-43.

Liao, J., Aggarwal, V. S., Nowotschin, S., Bondarev, A., Lipner, S. and Morrow, B. E. (2008). Identification of downstream genetic pathways of Tbx1 in the second heart field. *Dev. Biol.* **316**, 524-537.

Lindsay, E. A. (2001). Chromosomal microdeletions: dissecting del22q11 syndrome. *Nat. Rev. Genet.* **2**, 858-868.

Lindsay, E. A. and Baldini, A. (2001). Recovery from arterial growth delay reduces penetrance of cardiovascular defects in mice deleted for the DiGeorge syndrome region. *Hum. Mol. Genet.* **10**, 997-1002.

Lindsay, E. A., Botta, A., Jurecic, V., Carattini-Rivera, S., Cheah, Y. C., Rosenblatt, H. M., Bradley, A. and Baldini, A. (1999). Congenital heart disease in mice deficient for the DiGeorge syndrome region. *Nature* **401**, 379-383.

Lindsay, E. A., Vitelli, F., Su, H., Morishima, M., Huynh, T., Pramparo, T., Jurecic, V., Ogunrinu, G., Sutherland, H. F., Scambler, P. J. et al. (2001). Tbx1 haploinsufficiency in the DiGeorge syndrome region causes aortic arch defects in mice. *Nature* **410**, 97-101.

Liu, A., Losos, K. and Joyner, A. L. (1999). FGF8 can activate Gbx2 and transform regions of the rostral mouse brain into a hindbrain fate. *Development* **126**, 4827-4838.

Macatee, T. L., Hammond, B. P., Arenkiel, B. R., Francis, L., Frank, D. U. and Moon, A. M. (2003). Ablation of specific expression domains reveals discrete functions of ectoderm- and endoderm-derived FGF8 during cardiovascular and pharyngeal development. *Development* **130**, 6361-6374.

Merscher, S., Funke, B., Epstein, J. A., Heyer, J., Puech, A., Lu, M. M., Xavier, R. J., Demay, M. B., Russell, R. G., Factor, S. et al. (2001). TBX1 is responsible for cardiovascular defects in velo-cardio-facial/DiGeorge syndrome. *Cell* **104**, 619-629.

Meyers, E. N., Lewandoski, M. and Martin, G. R. (1998). An Fgf8 mutant allelic series generated by Cre- and Flp-mediated recombination. *Nat. Genet.* **18**, 136-141.

Mitchell, P. J., Timmons, P. M., Hebert, J. M., Rigby, P. W. and Tjian, R. (1991). Transcription factor AP-2 is expressed in neural crest cell lineages during mouse embryogenesis. *Genes Dev.* **5**, 105-119.

Miyagawa-Tomita, S., Waldo, K., Tomita, H. and Kirby, M. L. (1991). Temporospatial study of the migration and distribution of cardiac neural crest in quail-chick chimeras. *Am. J. Anat.* **192**, 79-88.

Nagy, A., Gertsenstein, M., Vintersten, K. and Behringer, R. (2003). *Manipulating The Mouse Embryo: A Laboratory Manual*, 3rd edn. Cold Spring Harbor, NY: Cold Spring Harbor Laboratory Press.
Nishibatake, M., Kirby, M. L. and van Mierop, L. H. (1987). Pathogenesis of persistent truncus arteriosus and dextroposed aorta in the chick embryo after neural crest ablation. *Circulation* **75**, 255-264.
Park, K. W., Morrison, C. M., Sorensen, L. K., Jones, C. A., Rao, Y., Chien, C. B., Wu, J. Y., Urness, L. D. and Li, D. Y. (2003). Robo4 is a vascular-specific receptor that inhibits endothelial migration. *Dev. Biol.* **261**, 251-267.
Paylor, R., Glaser, B., Mupo, A., Ataliotis, P., Spencer, C., Sobotka, A., Sparks, C., Choi, C. H., Oghalai, J., Curran, S. et al. (2006). Tbx1 haploinsufficiency is linked to behavioral disorders in mice and humans: implications for 22q11 deletion syndrome. *Proc. Natl. Acad. Sci. USA* **103**, 7729-7734.
Peirson, S. N., Butler, J. N. and Foster, R. G. (2003). Experimental validation of novel and conventional approaches to quantitative real-time PCR data analysis. *Nucleic Acids Res.* **31**, e73.
Plachez, C., Andrews, W., Liapi, A., Knoell, B., Drescher, U., Mankoo, B., Zhe, L., Mambetisaeva, E., Annan, A., Bannister, L. et al. (2008). Robos are required for the correct targeting of retinal ganglion cell axons in the visual pathway of the brain. *Mol. Cell. Neurosci.* **37**, 719-730.
Plump, A. S., Erskine, L., Sabatier, C., Brose, K., Epstein, C. J., Goodman, C. S., Mason, C. A. and Tessier-Lavigne, M. (2002). Slit1 and Slit2 cooperate to prevent premature midline crossing of retinal axons in the mouse visual system. *Neuron* **33**, 219-232.
Rao, M. S. and Anderson, D. J. (1997). Immortalization and controlled in vitro differentiation of murine multipotent neural crest stem cells. *J. Neurobiol.* **32**, 722-746.
Roberts, C., Ivins, S., Cook, A. C., Baldini, A. and Scambler, P. J. (2006). Cyp26 genes a1, b1 and c1 are down-regulated in Tbx1 null mice and inhibition of Cyp26 enzyme function produces a phenocopy of DiGeorge Syndrome in the chick. *Hum. Mol. Genet.* **15**, 3394-3410.
Schwarz, Q., Vieira, J. M., Howard, B., Eickholt, B. J. and Ruhrberg, C. (2008). Neuropilin 1 and 2 control cranial gangliogenesis and axon guidance through neural crest cells. *Development* **135**, 1605-1613.
Sheldon, H., Andre, M., Legg, J. A., Heal, P., Herbert, J. M., Sainson, R., Sharma, A. S., Kitajewski, J. K., Heath, V. L. and Bicknell, R. (2009). Active involvement of Robo1 and Robo4 in filopodia formation and endothelial cell motility mediated via WASP and other actin nucleation-promoting factors. *FASEB J.* **23**, 513-522.
Soriano, P. (1999). Generalized lacZ expression with the ROSA26 Cre reporter strain. *Nat. Genet.* **21**, 70-71.
Srivastava, D. and Olson, E. N. (2000). A genetic blueprint for cardiac development. *Nature* **407**, 221-226.
Stalmans, I., Lambrechts, D., De, S. F., Jansen, S., Wang, J., Maity, S., Kneer, P., von der, O. M., Swillen, A., Maes, C. et al. (2003). VEGF: a modifier of the del22q11 (DiGeorge) syndrome? *Nat. Med.* **9**, 173-182.
Stoller, J. Z. and Epstein, J. A. (2005). Identification of a novel nuclear localization signal in Tbx1 that is deleted in DiGeorge syndrome patients harboring the 1223delC mutation. *Hum. Mol. Genet.* **14**, 885-892.
Sundaresan, V., Mambetisaeva, E., Andrews, W., Annan, A., Knoll, B., Tear, G. and Bannister, L. (2004). Dynamic expression patterns of Robo (Robo1 and Robo2) in the developing murine central nervous system. *J. Comp. Neurol.* **468**, 467-481.
Suzuki, H. R. and Kirby, M. L. (1997). Absence of neural crest cell regeneration from the postotic neural tube. *Dev. Biol.* **184**, 222-233.
Taddei, I., Morishima, M., Huynh, T. and Lindsay, E. A. (2001). Genetic factors are major determinants of phenotypic variability in a mouse model of the DiGeorge/del22q11 syndromes. *Proc. Natl. Acad. Sci. USA* **98**, 11428-11431.
Tamada, A., Kumada, T., Zhu, Y., Matsumoto, T., Hatanaka, Y., Muguruma, K., Chen, Z., Tanabe, Y., Torigoe, M., Yamauchi, K. et al. (2008). Crucial roles of Robo proteins in midline crossing of cerebellofugal axons and lack of their up-regulation after midline crossing. *Neural Dev.* **3**, 29.
Teng, L., Mundell, N. A., Frist, A. Y., Wang, Q. and Labosky, P. A. (2008). Requirement for Foxd3 in the maintenance of neural crest progenitors. *Development* **135**, 1615-1624.
Toyofuku, T., Yoshida, J., Sugimoto, T., Yamamoto, M., Makino, N., Takamatsu, H., Takegahara, N., Suto, F., Hori, M., Fujisawa, H. et al. (2008). Repulsive and attractive semaphorins cooperate to direct the navigation of cardiac neural crest cells. *Dev. Biol.* **321**, 251-262.
Trainor, P. A. (2005). Specification of neural crest cell formation and migration in mouse embryos. *Semin. Cell Dev. Biol.* **16**, 683-693.
Trainor, P. and Krumlauf, R. (2000). Plasticity in mouse neural crest cells reveals a new patterning role for cranial mesoderm. *Nat. Cell Biol.* **2**, 96-102.
Vitelli, F., Morishima, M., Taddei, I., Lindsay, E. A. and Baldini, A. (2002a). Tbx1 mutation causes multiple cardiovascular defects and disrupts neural crest and cranial nerve migratory pathways. *Hum. Mol. Genet.* **11**, 915-922.
Vitelli, F., Taddei, I., Morishima, M., Meyers, E. N., Lindsay, E. A. and Baldini, A. (2002b). A genetic link between Tbx1 and fibroblast growth factor signaling. *Development* **129**, 4605-4611.
Wassarman, K. M., Lewandoski, M., Campbell, K., Joyner, A. L., Rubenstein, J. L., Martinez, S. and Martin, G. R. (1997). Specification of the anterior hindbrain and establishment of a normal mid/hindbrain organizer is dependent on Gbx2 gene function. *Development* **124**, 2923-2934.
Wilkinson, D. (1992). *In Situ Hybridisation: A Practical Approach*. Oxford: IRL Press.
Xu, H., Morishima, M., Wylie, J. N., Schwartz, R. J., Bruneau, B. G., Lindsay, E. A. and Baldini, A. (2004). Tbx1 has a dual role in the morphogenesis of the cardiac outflow tract. *Development* **131**, 3217-3227.
Xu, H., Cerrato, F. and Baldini, A. (2005). Timed mutation and cell-fate mapping reveal reiterated roles of Tbx1 during embryogenesis, and a crucial function during segmentation of the pharyngeal system via regulation of endoderm expansion. *Development* **132**, 4387-4395.
Xu, H., Viola, A., Zhang, Z., Gerken, C. P., Lindsay-Illingworth, E. A. and Baldini, A. (2007). Tbx1 regulates population, proliferation and cell fate determination of otic epithelial cells. *Dev. Biol.* **302**, 670-682.
Yagi, H., Furutani, Y., Hamada, H., Sasaki, T., Asakawa, S., Minoshima, S., Ichida, F., Joo, K., Kimura, M., Imamura, S. et al. (2003). Role of TBX1 in human del22q11.2 syndrome. *Lancet.* **362**, 1366-1373.
Yamagishi, H., Maeda, J., Hu, T., McAnally, J., Conway, S. J., Kume, T., Meyers, E. N., Yamagishi, C. and Srivastava, D. (2003). Tbx1 is regulated by tissue-specific forkhead proteins through a common Sonic hedgehog-responsive enhancer. *Genes Dev.* **17**, 269-281.
Yuan, W., Zhou, L., Chen, J. H., Wu, J. Y., Rao, Y. and Ornitz, D. M. (1999). The mouse SLIT family: secreted ligands for ROBO expressed in patterns that suggest a role in morphogenesis and axon guidance. *Dev. Biol.* **212**, 290-306.
Zhang, Z. and Baldini, A. (2008). In vivo response to high-resolution variation of Tbx1 mRNA dosage. *Hum. Mol. Genet.* **17**, 150-157.
Zhang, Z., Cerrato, F., Xu, H., Vitelli, F., Morishima, M., Vincentz, J., Furuta, Y., Ma, L., Martin, J. F., Baldini, A. et al. (2005). Tbx1 expression in pharyngeal epithelia is necessary for pharyngeal arch artery development. *Development* **132**, 5307-5315.
Zhang, Z., Huynh, T. and Baldini, A. (2006). Mesodermal expression of Tbx1 is necessary and sufficient for pharyngeal arch and cardiac outflow tract development. *Development* **133**, 3587-3595.
Zmojdzian, M., Da, Ponte, J. P. and Jagla, K. (2008). Cellular components and signals required for the cardiac outflow tract assembly in Drosophila. *Proc. Natl. Acad. Sci. USA* **105**, 2475-2480.